Science
AAAS

Actin Network Architecture Can Determine Myosin Motor Activity
Anne-Cécile Reymann *et al.*
Science **336**, 1310 (2012);
DOI: 10.1126/science.1221708

Science (print ISSN 0036-8075; online ISSN 1095-9203) is published weekly, except the last week in December, by the American Association for the Advancement of Science, 1200 New York Avenue NW, Washington, DC 20005.

consumption and energy production, particularly in *pink1*^{B9} mutants.

Our data predict that vitamin K_2 may also alleviate the defects in other conditions that impair mitochondrial function. We thus placed flies that express RNAi to different complex I components, *sbo* mutants that produce less ubiquinone, and rotenone-treated animals on control medium or on MK-4 medium and assessed Ψ_m and ATP levels. MK-4 rescued the mitochondrial defects in all of these flies (fig. S11, A and B). These results thus support a role for vitamin K_2 in the transport of electrons in eukaryotic mitochondria to produce ATP, similar to its role in prokaryotic membranes (*16*), suggesting that vitamin K_2 serves a conserved function in prokaryotes and mitochondria. Because mitochondria are involved in aging (*21*), we reared aged flies on MK-4 or overexpressed Heix but did not observe a significant rescue in mobility (fig. S11C). We surmise that long-lasting compensatory changes may be more important in these situations.

Human *UBIAD1* mutations may also affect mitochondrial function. Electron microscopic analyses of corneal samples from Schnyder's crystalline corneal dystrophy patients who harbor mutations in the *UBIAD1* gene (*22*–*24*) indicate cystic swelling of mitochondria, but the nature for this defect is unknown (*25*). Heix/UBIAD1 produces vitamin K_2, and in our studies vitamin K_2 rescued mitochondrial defects in numerous conditions that affect mitochondrial function. Vitamin K_2 was even effective at improving systemic locomotion defects in fully developed adult *pink1* and *parkin* mutant flies. Vitamin K_2 did not affect mitochondrial remodeling directly, but, by increasing ETC efficiency, it contributed to the proton motif force that facilitates ATP production, similar to ubiquinone (*26*). Vitamin K_2 may thus constitute a promising compound to treat mitochondrial pathology, also in PD patients suffering from Pink1 or Parkin deficiency.

References and Notes

1. M. Vila, S. Przedborski, *Nat. Med.* **10** (suppl.), S58 (2004).
2. W. Mandemakers, V. A. Morais, B. De Strooper, *J. Cell Sci.* **120**, 1707 (2007).
3. E. M. Valente *et al.*, *Science* **304**, 1158 (2004); 10.1126/science.1096284.
4. I. E. Clark *et al.*, *Nature* **441**, 1162 (2006).
5. J. Park *et al.*, *Nature* **441**, 1157 (2006).
6. V. A. Morais *et al.*, *EMBO Mol. Med.* **1**, 99 (2009).
7. P. Verstreken *et al.*, *Neuron* **63**, 203 (2009).
8. P. R. Hiesinger *et al.*, *Cell* **121**, 607 (2005).
9. V. Uytterhoeven, S. Kuenen, J. Kasprowicz, K. Miskiewicz, P. Verstreken, *Cell* **145**, 117 (2011).
10. Materials and methods are available as supplementary materials on *Science* Online.
11. S. Vilain *et al.*, *PLoS Genet.* **8**, e1002456 (2012).
12. K. Suvarna, D. Stevenson, R. Meganathan, M. E. S. Hudspeth, *J. Bacteriol.* **180**, 2782 (1998).
13. K. Nakagawa *et al.*, *Nature* **468**, 117 (2010).
14. J. M. Conly, K. Stein, L. Worobetz, S. Rutledge-Harding, *Am. J. Gastroenterol.* **89**, 915 (1994).
15. H. Deng, M. W. Dodson, H. Huang, M. Guo, *Proc. Natl. Acad. Sci. U.S.A.* **105**, 14503 (2008).
16. E. C. C. Lin, D. Kuritzkes, in Escherichia coli *and* Salmonella typhimurium: *Cellular and Molecular Biology*, F. C. Neidhardt *et al.*, Eds. (American Society for Microbiology, Washington, DC, 1987), pp. 202–221.
17. M. L. Nickerson *et al.*, *PLoS ONE* **5**, e10760 (2010).
18. H. H. Thijssen, M. J. Drittij-Reijnders, *Br. J. Nutr.* **72**, 415 (1994).
19. Y. Usui *et al.*, *J. Chromatogr.* **489**, 291 (1989).
20. B. de Paepe *et al.*, *Pediatr. Res.* **59**, 2 (2006).
21. S. L. Hebert, I. R. Lanza, K. S. Nair, *Mech. Ageing Dev.* **131**, 451 (2010).
22. A. Orr *et al.*, *PLoS ONE* **2**, e685 (2007).
23. V. S. Yellore *et al.*, *Mol. Vis.* **13**, 1777 (2007).
24. J. S. Weiss *et al.*, *Invest. Ophthalmol. Vis. Sci.* **48**, 5007 (2007).
25. A. Garner, R. C. Tripathi, *Br. J. Ophthalmol.* **56**, 400 (1972).
26. S. McCarthy, M. Somayajulu, M. Sikorska, H. Borowy-Borowski, S. Pandey, *Toxicol. Appl. Pharmacol.* **201**, 21 (2004).

Acknowledgments: We thank H. Bellen, J. Park, J. Chung, the Bloomington *Drosophila* stock center, and the Yale *E. coli* stock center. Support was provided by an Agentschap voor Innovatie door Wetenschap en Technologie (IWT)–Vlaanderen to M.V., a European Research Council Starting Grant (no. 260678), Fonds Voor Wetenschappelijk Onderzoek (G074709-G095511-G094011), the Research Fund KU Leuven, a Methusalem grant, KU Leuven, the Hercules and Francqui foundations, and VIB. The data reported in this paper are tabulated in the main paper and in the supplementary materials. B.D.S. is a paid consultant for Janssen Pharmaceutica (Johnson and Johnson) with regard to Alzheimer's disease and Parkinson's disease.

Supplementary Materials

www.sciencemag.org/cgi/content/full/science.1218632/DC1
Materials and Methods
Figs. S1 to S11
References (*27*–*44*)

3 January 2012; accepted 13 April 2012
Published online 10 May 2012;
10.1126/science.1218632

Actin Network Architecture Can Determine Myosin Motor Activity

Anne-Cécile Reymann,[1] Rajaa Boujemaa-Paterski,[1] Jean-Louis Martiel,[1] Christophe Guérin,[1] Wenxiang Cao,[2] Harvey F. Chin,[2]* Enrique M. De La Cruz,[2] Manuel Théry,[1]† Laurent Blanchoin[1]†

The organization of actin filaments into higher-ordered structures governs eukaryotic cell shape and movement. Global actin network size and architecture are maintained in a dynamic steady state through regulated assembly and disassembly. Here, we used experimentally defined actin structures in vitro to investigate how the activity of myosin motors depends on network architecture. Direct visualization of filaments revealed myosin-induced actin network deformation. During this reorganization, myosins selectively contracted and disassembled antiparallel actin structures, while parallel actin bundles remained unaffected. The local distribution of nucleation sites and the resulting orientation of actin filaments appeared to regulate the scalability of the contraction process. This "orientation selection" mechanism for selective contraction and disassembly suggests how the dynamics of the cellular actin cytoskeleton can be spatially controlled by actomyosin contractility.

Actin filament networks comprise a large variety of different structures. Their spatial organization supports complex cell-shape regulation. The dynamics and mechanical properties of these structures result from the assembly of polarized actin filaments. Filopodia, retraction fibers, and centripetal fibers are built of parallel filaments (*1*, *2*). Stress fibers and transverse arcs have filaments arranged in antiparallel orientations (*3*, *4*). The lamellipodium is a dense array of branched filaments (*5*).

The global architecture of the actin cytoskeleton is maintained through coordinated actions of a large number of regulatory proteins that modulate filament assembly and disassembly (*6*), as well as through contractility driven by myosin motor proteins (*7*). Myosin motor proteins can also promote filament disassembly (*8*). Collectively, these observations have supported a mechanism in which the coupling between myosin contractility and filament disassembly ensures a temporal synchrony between actin retrograde flow at the front and filament disassembly at the rear of migrating cells (*9*).

Central to this coupling mechanism is that filaments are selected for contraction or disassembly, but it is not known what factors determine the response to myosin contractile forces (*10*). Here, we used micropatterning methods to assemble geometrically controlled and polarized actin filament networks (*11*) to evaluate how the overall polarity of actin filament architectures determines their response—reorganization and/or disassembly—to myosin contractile forces.

Actin filament growth on bar-shaped micropatterns covered with the Wiskott-Aldrich syn-

[1]Institut de Recherches en Technologies et Sciences pour le Vivant (iRTSV), Laboratoire de Physiologie Cellulaire et Végétale, Centre National de la Recherche Scientifique (CNRS)–Commissariat à l'Energie Atomique et aux Energies Alternatives (CEA)–Institut National de la Recherche Agronomique (INRA)–Université Joseph Fourier (UJF), Grenoble, 38054, France. [2]Department of Molecular Biophysics and Biochemistry, Yale University, New Haven, CT 06520, USA.

*Present address: Department of Biochemistry, Weill Cornell Medical College, New York, NY 10065, USA.
†To whom correspondence should be addressed: manuel.thery@cea.fr (M.T.); laurent.blanchoin@cea.fr (L.B.)

drome protein pWA domain, an actin-promoting factor, leads to the formation of a dense meshwork on the micropatterned region and parallel array of filaments with barbed ends oriented away from the nucleation site out of this region (*11*) (movie S1). Addition of myosins to the polymerization mix—including Arp2/3 complex, profilin, and actin monomers—allowed us to investigate the contraction of this network (fig. S1). We used double-headed (HMM) myosin VI (*12*), a processive pointed end–directed motor that could sustain continuous force and motility without the need for self-assembly into minifilaments.

Green fluorescent protein (GFP)–tagged myosins and Alexa 568–labeled actin monomers allowed real-time tracking of actin growth and myosin-induced reorganization (Fig. 1). Myosins associated with the network and induced a clear two-phase process constituted by the deformation of actin networks followed by a massive filament disassembly of the condensed central meshwork (Fig. 1A and movie S2, short bars). Depending on the geometry of the pattern, this two-phase process could lead to the formation of a disassembly wave (fig. S2, long bars). We then tested if a barbed end–directed myosin had a similar effect on network reorganization. Muscle myosin II bipolar filaments induced a two-phase deformation-disassembly of the network similar to that caused by myosin VI, although the extent of deformation before disassembly was local and less pronounced (Fig. 1B and movie S3), presumably because of resistance from filament cross-linking (*13*). Consistent with this interpretation, the actin filament cross-linker, α-actinin, also minimized myosin VI–induced macroscopic deformation before network disassembly (Fig. 1C, fig. S3, and movie S4). Varying myosin concentration revealed that deformation and disassembly occurred above different concentration thresholds depending on the reticulated actin network (fig. S3).

Parallel and polarized filaments emerging from the micropatterned regions with their barbed ends oriented outward (*11*) did not contract and disassemble with either myosin VI or II (Fig. 1, A and B, and movies S2 and S3). Perhaps networks composed of randomly oriented filaments can contract and disassemble, whereas parallel filament arrays cannot. To understand the contribution of actin filaments' polarity during actomyosin contraction, we used evanescent wave microscopy to follow in real time the effect of myosin on a growing branched network (fig. S4 and movie S5). Networks did not contract in the presence of myosin VI when they remained as individual patches of branched and parallel filaments. When individual subnetworks interacted in antiparallel orientation, myosin rapidly induced a deformation of the network by its alignment into antiparallel bundles (fig. S4 and movie S5).

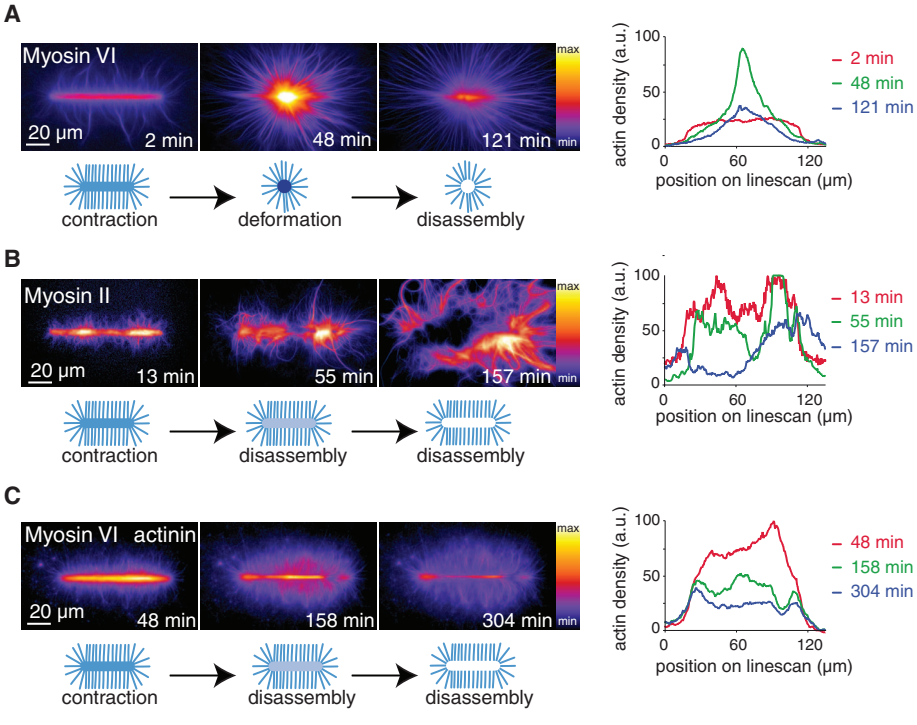

Fig. 1. Myosin-induced actin meshwork contraction and disassembly. (**A**) Time series of myosin VI–induced network contraction on a bar-shaped micropattern. Actin filaments were visualized with fluorescent monomers. "Fire" look-up table color-coding reveals variations in actin network densities, quantified with a line scan along the bar at different time points. Actin density peaks because of network deformation after 48 min then falls off because of network disassembly. (**B**) Same as (A) with muscle myosin II–induced contraction. (**C**) Same as (A) with 100 nM α-actinin in the polymerization mix.

This "orientation selection" for selective contraction and disassembly of antiparallel filaments by myosin was further tested on networks of controlled polarity and architecture. Filaments nucleated on an eight-branch radial array lead to the formation of all the diversity in actin organization found in a cell, a meshwork of branched and randomly oriented actin filaments on the micropattern, bundles of aligned antiparallel filaments in the most central part of the array, and bundles of aligned parallel filaments in the distal part of the array (*11*) (Fig. 2A). This defined distinction between zones containing parallel, antiparallel, or branched filament organizations (Fig. 2G) enabled us to characterize the region-selectivity of myosin-induced reorganization. Myosin VI was chosen to induce contraction forces on these actin architectures because it is a pointed end–oriented motor and can pull on filaments with their barbed ends pointing out of the micropatterns (fig. S5 and movie S6). The addition of myosin VI in solution led to the rapid contraction of the antiparallel bundles and branched meshwork, followed by their disassembly (Fig. 2B, central black hole after 1640 s; Fig. 2, C and D; and movies S7 and S8). The parallel bundles remained unperturbed and continued to elongate until the monomers freshly released by central disassembly were consumed (Fig. 2, D and E, and movie S8), although myosins were present on these bundles (Fig. 2F) on which they could move (fig. S6). These processes could also be monitored on larger structures in which antiparallel networks were easier to visualize (fig. S7). Thus, myosin-induced contraction is specific to bundles of antiparallel filaments and branched meshwork, and myosin-induced disassembly of these structures further supplies actin monomers for the growth of parallel filament bundles (Fig. 2G).

Next, we further characterized the contraction properties of bundles of antiparallel filaments and branched meshwork. We compared the effect of myosins on actin rings in which the proportion of antiparallel filaments zones were finely controlled (Fig. 3A). Filaments assemble into branched meshwork on full rings (Fig. 3A). On dotted rings, filaments formed branched meshwork on the dots but specifically formed bundles of antiparallel filaments between the dots (Fig. 3A). The proportion of bundles of antiparallel filaments thus scales inversely with the number of dots in constant-sized rings. We monitored actin network contraction and deformation upon the addition of myosin (Fig. 3B and movie S9). We measured the fluorescence intensity of actin and myosin in all angular sectors of the rings during contraction (Fig. 3, C and D). Myosins first accumulated on the actin network without generating global deformation (Fig. 3D, green curve before time 0). Above a critical accumulation of myosins, deformation started (Fig. 3D, blue curve time 0). Network deformation was coupled to network disassembly

(Fig. 3D, red curve). In addition, the total amounts of actin and myosin decreased following a decay pattern similar to that of the radius of both full and dotted rings (Fig. 3D). As a consequence, the density of actin was constant during contraction (fig. S8). Each sector of the rings followed three distinct phases during remodeling (Fig. 3E): first, a delay phase during which filaments were aligned; second, a fast-contraction phase with a constant rate; and finally, a third phase during which the network was highly compacted at the ring center and the contraction slowed down. We measured the rate of the fast-contraction phase, because it reflects the main amplitude of change in sector size. We compared the contraction rates of rings with continuous or dotted nucleating regions. Dot number and spacing were chosen to vary the ratio r between the total length of branched meshwork, $P_{branched}$ (P_b or Pb on figures), and the ring's perimeter, P. The contraction rate increased significantly as the ratio r decreased (Fig. 3F and movie S10). Thus, for a given actin structure, the contraction rate is determined by the relative proportions of antiparallel bundles and branched meshwork.

The contraction rate of an in vivo structure, such as the cytokinetic ring, increases in proportion to its size, a process termed scalability, although no molecular determinants of the underlying mechanism have been established (*14*, *15*). To evaluate the respective contributions of ring size and composition to the contraction rate, we varied the ring perimeter P and the portion of this perimeter that nucleates a branched meshwork P_b independently (Fig. 4A and movie S11). When P and P_b increased equally, the contraction rate was unaffected, although the ring size increased (see black and blue rings in Fig. 4A). Thus, no scalability is observed when the proportion of antiparallel bundles and branched meshwork is maintained constant during size increase. When P was increased and P_b kept constant, the contraction rate increased (see the pairs: black, red rings and green, blue rings in Fig. 4A). Scalability is thus only observed when the size increase of the actin structure is coupled to an increase of the proportion of antiparallel bundles.

These results demonstrate that contraction rate variations result from the proportion of antiparallel filament bundles, which is controlled by the size of and distance between nucleation regions. In all conditions tested, the velocity, V, was proportional to the ratio P/P_b (fig. S9). These observations could be captured by a simple physical model in which the contraction force was proportional to the amount of myosins per unit length of filament, and the friction drag was proportional to the length of branched meshwork (Fig. 4B). In this model, network disassembly by myosins plays a passive role because it simply prevents the elastic reaction, which could arise from network compaction during contraction, but a more active role of network disassembly during contraction remains possible.

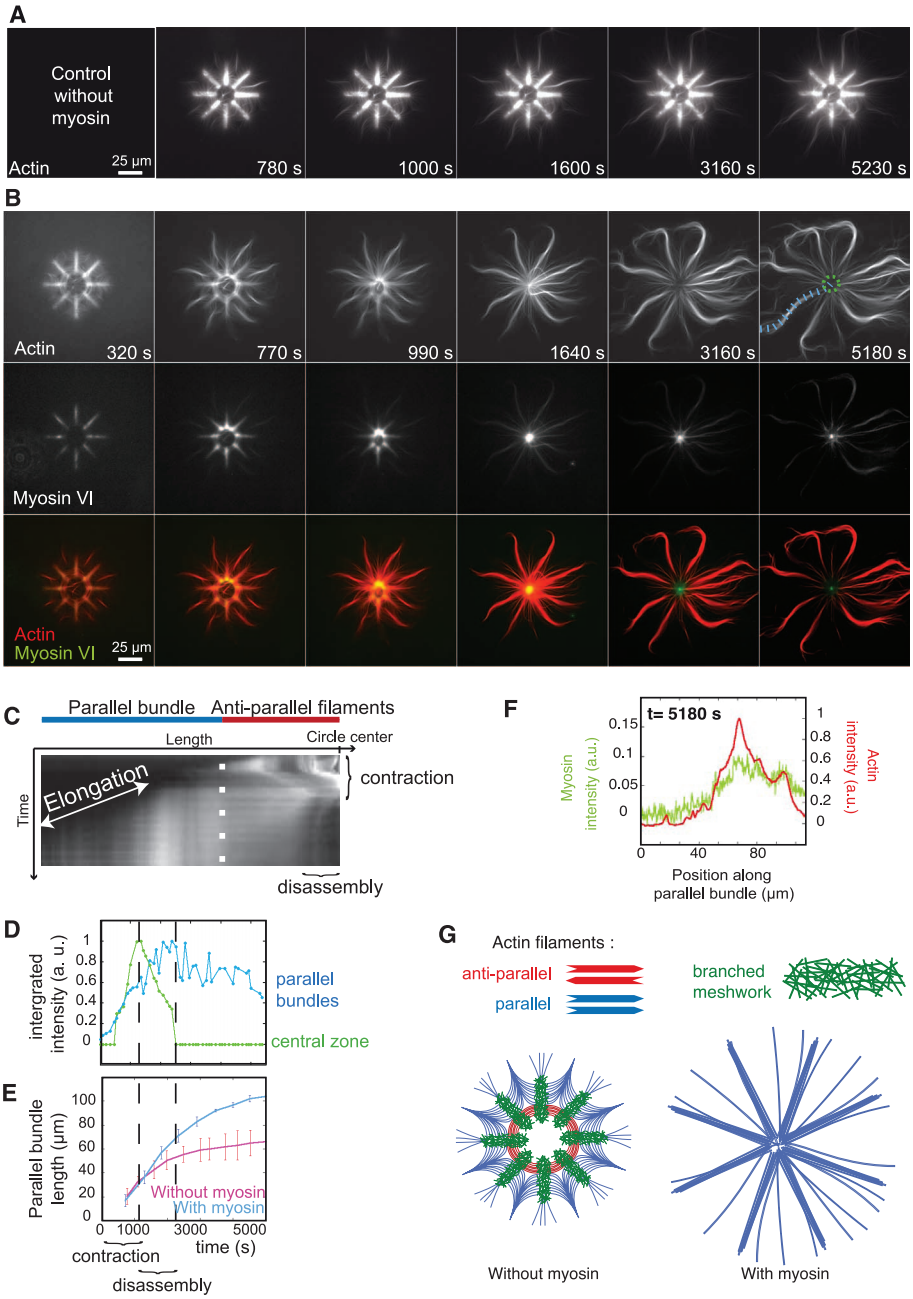

Fig. 2. Regioselective action of myosins. (**A**) Time series of network assembly on an eight-branch actin-nucleating radial array. (**B**) Time series of myosin VI–induced architecture selective contraction and disassembly (actin, myosin, and an overlay are shown). (**C**) Kymograph of actin fluorescence along a parallel bundle [blue dashed line in (B) 5180 s] and central region of actin filaments [dashed green circle in (B) 5180 s], showing the different localization of elongation and contraction and of disassembly. (**D**) Fluorescence intensity of a central zone [dashed green circle in (B)] and a parallel bundle [blue dashed line in (B)] over time. (**E**) Length variations of parallel bundles over time in the absence or presence of myosins. (**F**) Line scan of fluorescence intensity along a parallel bundle confirming myosin presence all along. (**G**) Schematic representation of the final architecture on an eight-branch actin-nucleating radial array in the absence or presence of myosins in solution.

Thus, myosins act on actin networks in a manner that depends on the actin filament orientation. Parallel filaments align and elongate, whereas antiparallel filaments contract and disassemble. We term such rules in myosin selectivity an "orientation selection" mechanism that should not induce a global cell collapse but should instead support the overall spatial coordination of different actin structures by regulating their specific reorientation, deformation, and disassembly.

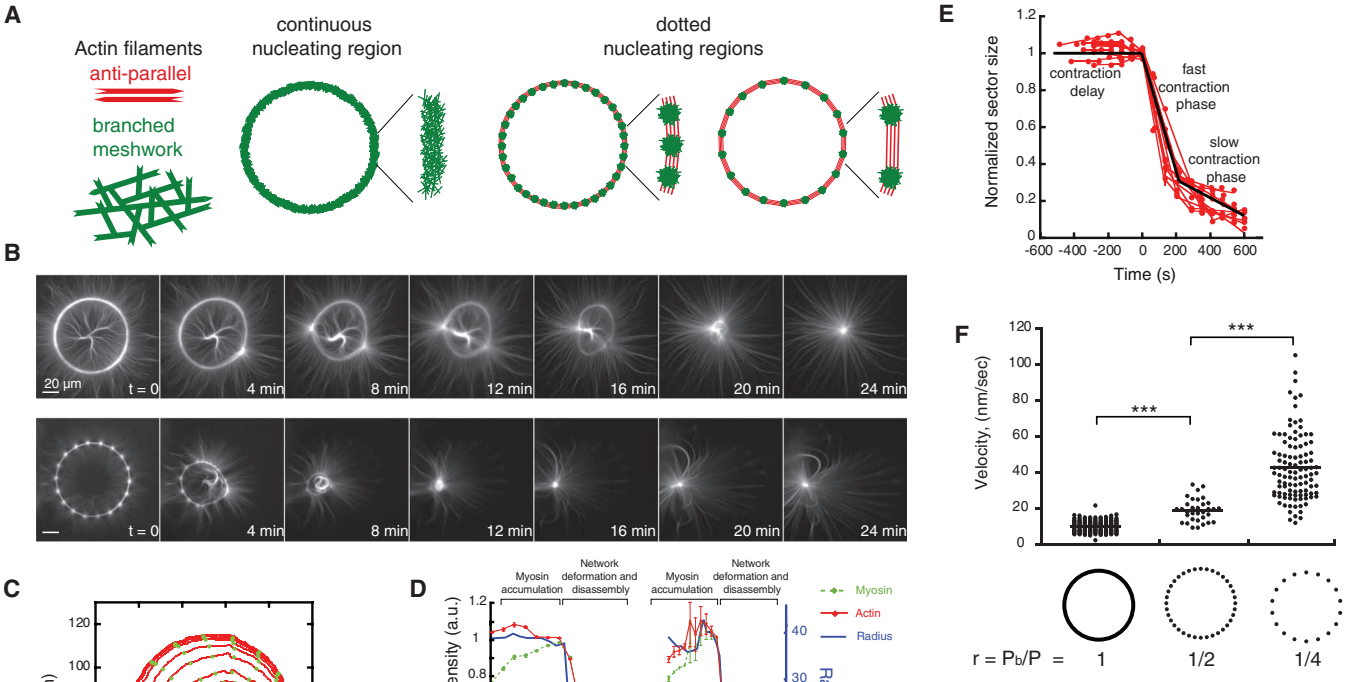

Fig. 3. The proportion of antiparallel filaments regulates network contraction rate. (**A**) Schematic representation of actin networks nucleated on full and dotted rings. (**B**) Time series of myosin-induced contraction of actin networks nucleated from full (top) and dotted (bottom) rings. (**C**) Illustration of automated network contraction analysis (see materials and methods). Each circle represents a time point. (**D**) The radius and total fluorescence intensities of both actin and myosin were recorded for all angular sectors over time. (**E**) Ring constriction kinetics. Time series of length values (red dots) could be fitted by three distinct phases (black line). (**F**) Fast-contraction phase velocity measurements were compared among various ring compositions.

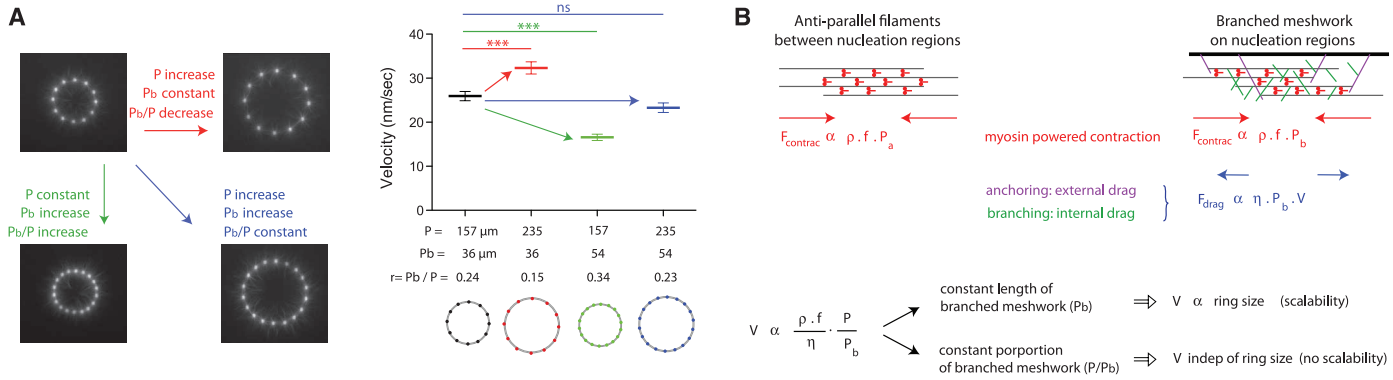

Fig. 4. The proportion of branched meshwork regulates the scalability of ring contraction. (**A**) Respective effects of size and proportion of branched meshwork in contraction kinetics. We varied the ring perimeter P and the length of that perimeter nucleating a branched meshwork P_b independently. Images show an early time point during actin network assembly on micropatterned dots. Fast-contraction phase velocity measurements were compared among various ring configurations. (**B**) Model description. Filaments assemble into antiparallel bundles between nucleation regions (left scheme). Nucleation regions (wide black bar, right scheme) generate branched actin meshwork. The contraction force is proportional to the density of myosins per unit length of filament, ρ, to the force per myosin head, f, and to the portion of the perimeter made of the relevant network, P_a for the antiparallel bundles and P_b for the branched meshwork. Myosin density is constant over the entire perimeter $P = P_a + P_b$. Antiparallel bundles have a friction drag negligible compared with that of the branched meshwork in which the effective friction coefficient, η, has two origins: an external drag due to network anchoring on the nucleation region and an internal drag due to entanglement of filament branches. The balance between the total contraction force and the frictional drag sets the contraction velocity V, which appeared to be proportional to the ratio P/P_b as observed in all our experiments.

References and Notes

1. L. P. Cramer, T. J. Mitchison, *J. Cell Biol.* **131**, 179 (1995).
2. D. Vignjevic *et al.*, *J. Cell Biol.* **160**, 951 (2003).
3. L. P. Cramer, M. Siebert, T. J. Mitchison, *J. Cell Biol.* **136**, 1287 (1997).
4. A. B. Verkhovsky, T. M. Svitkina, G. G. Borisy, *J. Cell Biol.* **131**, 989 (1995).
5. T. M. Svitkina, A. B. Verkhovsky, K. M. McQuade, G. G. Borisy, *J. Cell Biol.* **139**, 397 (1997).
6. T. D. Pollard, G. G. Borisy, *Cell* **112**, 453 (2003).
7. C. Veigel, C. F. Schmidt, *Nat. Rev. Mol. Cell Biol.* **12**, 163 (2011).
8. L. Haviv, D. Gillo, F. Backouche, A. Bernheim-Groswasser, *J. Mol. Biol.* **375**, 325 (2008).
9. C. A. Wilson *et al.*, *Nature* **465**, 373 (2010).

10. C. M. Brawley, R. S. Rock, *Proc. Natl. Acad. Sci. U.S.A.* **106**, 9685 (2009).
11. A.-C. Reymann *et al.*, *Nat. Mater.* **9**, 827 (2010).
12. E. M. De La Cruz, E. M. Ostap, H. L. Sweeney, *J. Biol. Chem.* **276**, 32373 (2001).
13. G. H. Koenderink *et al.*, *Proc. Natl. Acad. Sci. U.S.A.* **106**, 15192 (2009).
14. A. Carvalho, A. Desai, K. Oegema, *Cell* **137**, 926 (2009).
15. M. E. Calvert *et al.*, *J. Cell Biol.* **195**, 799 (2011).

Acknowledgments: We thank C. Sykes and J. Faix for muscle myosin II protein, F. Senger for image analysis, and K. John for discussions regarding the computational model. This work was supported by grants from Human Frontier Science Program (RGP0004/2011 awarded to L.B. and E.M.D.L.C.), Agence Nationale de la Recherche (ANR-08-BLANC-0012 awarded to L.B.), Institut National du Cancer (INCA-2011-141 awarded to M.T.), NIH (GM097348 awarded to E.M.D.L.C.), and a Ph.D. Fellowship from the Irtelis program of the CEA (awarded to A.C.R.). E.M.D.L.C. is an American Heart Association Established Investigator, an NSF Career Award recipient (MCB-0546353), and a Hellman Family Fellow. The use of micropatterned substrates to control actin network self-assembly is protected by patent EP2011/063676. The data reported in this manuscript are tabulated in the main paper and in the supplementary materials.

Supplementary Materials
www.sciencemag.org/cgi/content/full/336/6086/1310/DC1
Materials and Methods
Figs. S1 to S9
References (*16*–*21*)
Movies S1 to S11

9 March 2012; accepted 1 May 2012
10.1126/science.1221708

Interactions Between Commensal Fungi and the C-Type Lectin Receptor Dectin-1 Influence Colitis

Iliyan D. Iliev,[1] Vincent A. Funari,[2,3] Kent D. Taylor,[2] Quoclinh Nguyen,[2] Christopher N. Reyes,[1] Samuel P. Strom,[2] Jordan Brown,[2] Courtney A. Becker,[1] Phillip R. Fleshner,[4] Marla Dubinsky,[1,5] Jerome I. Rotter,[2] Hanlin L. Wang,[6] Dermot P. B. McGovern,[1,2] Gordon D. Brown,[7] David M. Underhill[1,6,8*]

The intestinal microflora, typically equated with bacteria, influences diseases such as obesity and inflammatory bowel disease. Here, we show that the mammalian gut contains a rich fungal community that interacts with the immune system through the innate immune receptor Dectin-1. Mice lacking Dectin-1 exhibited increased susceptibility to chemically induced colitis, which was the result of altered responses to indigenous fungi. In humans, we identified a polymorphism in the gene for Dectin-1 (*CLEC7A*) that is strongly linked to a severe form of ulcerative colitis. Together, our findings reveal a eukaryotic fungal community in the gut (the "mycobiome") that coexists with bacteria and substantially expands the repertoire of organisms interacting with the intestinal immune system to influence health and disease.

Interactions between the commensal microflora and the gut immune system are critical for establishing a balance between immunity and tissue health. Changes in gut bacteria described as "dysbiosis" have been associated with intestinal inflammation (*1*–*3*) and metabolic syndrome (*4*–*6*). The vast majority of studies on commensal microbiota have focused on gut bacteria, and the terms "intestinal microbiota" and "intestinal bacteria" are often used interchangeably. Recent studies have begun to note, however, that a fraction of gut microorganisms are not bacterial (*7*). Although a few studies have suggested the presence of commensal fungi in the gut (*8*, *9*), whether they interact with the mucosal immune system or influence diseases is unknown.

Fungi are recognized by a number of immune receptors among which Dectin-1 has emerged as key for phagocytosis and killing by myeloid phagocytes. Dectin-1 is a C-type lectin receptor that recognizes β-1,3-glucans found in the cell walls of nearly all fungi. Dectin-1 activates intracellular signals through caspase recruitment domain–containing protein 9 (CARD9), which leads to inflammatory cytokine production and induction of T helper 17 (T_H17) immune responses (*10*–*13*). Deficiencies in either Dectin-1 or CARD9 result in enhanced susceptibility to pathogenic fungal infections in humans and mice (*14*–*16*). Polymorphic variants in the gene for CARD9 are strongly associated with Crohn's disease and ulcerative colitis in humans (*17*, *18*). Furthermore, anti–*Saccharomyces cerevisiae* antibodies (ASCA) against yeast mannan have been strongly associated with Crohn's disease (*19*, *20*). Together, these last-named findings suggest a possible link between immune responses to commensal fungi and intestinal disease.

We examined fungal distribution and detected fungal ribosomal DNA (rDNA) throughout the murine gastrointestinal tract with highest densities in the terminal colon of C57BL/6 (Fig. 1A) and 129S2/Sv (fig. S1A) mice. We stained colonic tissue sections and observed that fungi are abundant and in close proximity with commensal bacteria (Fig. 1B and figs. S1B and S2 to S4). Furthermore, we found that a soluble Dectin-1 probe (*21*) binds to 5 to 7% of the fecal material, consisting of fungal cells with various morphologies (Fig. 1C and fig. S5). Fungi were also present in rat, guinea pig, rabbit, pig, dog, and human feces (fig. S1C). Together, the data demonstrate that commensal fungi contribute to the intestinal microbial community in many species.

We next examined whether gut fungi can be detected by the immune system upon intestinal insult. We utilized a mouse model of dextran sodium sulfate (DSS)–induced colitis extended to allow antibody responses to develop. We found that DSS-induced intestinal inflammation led to the development of circulating immunoglobulin G (IgG) and IgM antibodies against fungi (ASCA) (Fig. 1D), which suggested that fungal antigens indigenous to the gut might be responsible for the induction of ASCA during colitis.

Because gut commensal fungi are recognized by Dectin-1, we tested whether Dectin-1–deficient mice (*Clec7a*$^{-/-}$) are susceptible to DSS-induced colitis. *Clec7a*$^{-/-}$ mice experienced increased weight loss (Fig. 2A) and displayed altered histology characterized by increased mucosal erosion, crypt destruction, inflammatory cell infiltration, and tumor necrosis factor–α (TNF-α) production in the colon (Fig. 2, B to D) as compared with their wild-type (WT) littermate controls. We further detected augmented production of interferon-γ (IFN-γ) and interleukin-17 (IL-17) in intestines from *Clec7a*$^{-/-}$ mice (fig. S6). Similar results were obtained comparing cohoused animals (fig. S7). These results indicate that Dectin-1 deficiency leads to increased susceptibility to colitis.

Many studies have documented the importance of bacteria in intestinal inflammation, so we examined whether bacteria could contribute to the susceptible phenotype. We observed no significant differences in major phyla of commensal bacteria between WT and *Clec7a*$^{-/-}$ mice (fig. S8). To directly determine whether microflora can transfer disease, we depleted intestinal bacteria and fungi with antibiotics, transplanted fecal microflora from WT or *Clec7a*$^{-/-}$ mice, and exposed mice to DSS. Microflora from *Clec7a*$^{-/-}$ mice did not transfer susceptibility to disease (Fig. 2, E and F, and figs. S9 and S10). The data demonstrate that the disease phenotype in the *Clec7a*$^{-/-}$ mice is affected by the genotype of the mouse, not by initial differences in microflora.

We know very little about what commensal fungi populate the murine gut or how they con-

[1]Inflammatory Bowel and Immunobiology Research Institute, Cedars-Sinai Medical Center, Los Angeles, CA 90048, USA. [2]Medical Genetics Institute, Cedars-Sinai Medical Center, Los Angeles, CA 90048, USA. [3]Department of Pediatrics, David Geffen School of Medicine, University of California, Los Angeles, CA 90095, USA. [4]Department of Surgery, Cedars-Sinai Medical Center, Los Angeles, CA 90048, USA. [5]Department of Pediatrics, Cedars-Sinai Medical Center, Los Angeles, CA 90048, USA. [6]Department of Pathology and Laboratory Medicine, David Geffen School of Medicine, University of California, Los Angeles, CA 90095, USA. [7]Section of Immunology and Infection, Division of Applied Medicine, Institute of Medical Sciences and The Aberdeen Fungal Group, University of Aberdeen, Aberdeen AB24 2ZD, UK. [8]Research Division of Immunology, Cedars-Sinai Medical Center, Los Angeles, CA 90048, USA.

*To whom correspondence should be addressed. E-mail: david.underhill@csmc.edu